ELSEVIER

Journal of Molecular Catalysis A: Chemical 131 (1998) 225–241

JOURNAL OF MOLECULAR CATALYSIS A: CHEMICAL

High pressure catalytic processes studied by infrared-visible sum frequency generation

Paul S. Cremer [a], Xingcai Su [b,c], Gabor A. Somorjai [b,c], Y. Ron Shen [b,d,*]

[a] *Department of Chemistry, Stanford University, Stanford, CA, USA*
[b] *Materials Sciences Division, Lawrence Berkeley National Laboratory, Berkeley, CA, USA*
[c] *Department of Chemistry, University of California at Berkeley, Berkeley, CA, USA*
[d] *Department of Physics, University of California at Berkeley, Berkeley, CA, USA*

Received 17 June 1997; accepted 18 September 1997

Abstract

The recent development of infrared-visible sum frequency generation (SFG), a surface-specific vibrational spectroscopy, has helped bridge the pressure gap between studies of heterogeneous catalysis under high vacuum and atmospheric pressure. This is achieved by in situ monitoring of surface species at high pressure via their SFG vibrational spectra and correlating the results with the simultaneously measured reaction rate using gas chromatography. Examples of systems studied include olefin hydrogenation and carbon monoxide oxidation over the (111) crystalline face of platinum. In these examples, the studies succeed in revealing the molecular details of the surface reactions. Identification of key intermediates and their concentrations has made it possible for the first time to calculate turn over rates per active surface species rather than just per exposed surface metal atom. In all cases, the key intermediate of the reaction is not detectable on the surface in UHV under similar temperatures. © 1998 Elsevier Science B.V.

Keywords: Sum frequency generation; Spectroscopy; Chromatography

1. Introduction

Over the past three decades, surface scientists have modeled heterogeneous catalytic reactions on metal single crystals by a variety of techniques [1]. Most of these involved using the arsenal of ultra high vacuum (UHV) compatible equipment (esp. electron spectroscopies) available to perform such studies under the pristine conditions of 10^{-10} Torr. These included low energy electron diffraction (LEED) for surface crystallography, high resolution electron energy loss spectroscopy (HREELS) and reflection adsorption infrared spectroscopy (RAIRS) for probing surface vibrational modes, Auger Electron Spectroscopy (AES) and X-ray photoemission spectroscopy (XPS) for chemical analysis of the surface, and mass spectrometry for monitoring the desorption of surface species. Much important information was obtained in terms of adsorbate ordering, adsorbate–adsorbate interactions, surface restructuring, surface diffusion, thermal decomposition, and specific active sites for reaction [2]. However, the surface species

* Corresponding author.

PII S1381-1169(97)00268-9

observed under UHV conditions are not necessarily the same as those present during reaction. Indeed, under UHV, one expects to see only strongly bound species as more weakly bound ones desorb quickly at all but the lowest temperatures. Hence, proper characterization of weakly bound species that may be key intermediates under ambient conditions is difficult if not impossible. Further, at high pressure, the surface coverage of some adsorbates is much greater than in vacuum. Since bonding is usually coverage dependent, this must be explored in a high pressure environment. Finally, it is difficult to guess which species are responsible for an ambient pressure reaction and by which pathway if the only results available are for systems 13 orders of magnitude below atmospheric pressure. Clearly, the pressure gap between the plethora of vacuum results obtained at 10^{-10} Torr and the characterization of reactions under realistic conditions (atmospheres of reactant gases) needs to be bridged.

To help bridge this gap, infrared-visible sum frequency generation (SFG), a surface specific nonlinear optical spectroscopy [3–6] has been employed to monitor transition metal surfaces over a wide range of temperatures (250–1000 K) and pressures (UHV to atmospheres). The use of SFG in combination with gas chromatography is extremely powerful. This is because vibrational spectroscopy can be performed simultaneously with kinetic measurements from gas phase analysis. SFG vibrational spectroscopy allows identification and quantification of surface species during reaction. On the other hand, gas chromatography permits quantification of all reactants and products, thus providing information on reaction rate. The object is to correlate reaction rates with the specific species present on the surface during catalytic reaction. In practice, the surface pretreatment, temperature, reactant gas pressures, transition metal, etc. are varied to observe their effects on the reaction rate and concentration of surface adsorbates. Such information may then be used to determine mechanistic pathways, specific reaction sites, and reaction rates with respect to concentrations of individual intermediates.

This review article will first give a description of the apparatus employed to connect nonlinear optical measurements with batch reactor studies. Considerations of applying SFG to the surface of single crystal metal catalysts will be discussed. Following this, we will give some specific examples of how this technique can be applied for in situ studies of catalytic surface reactions.

2. Experimental design

2.1. Apparatus

Fig. 1 shows the set-up for coupling SFG optics to a heterogeneous catalytic batch reaction cell. The batch reactor is fitted with optical windows and coupled via a gate valve to an UHV system. The reactor can be charged up to 1.2 atm of total pressure and includes a recirculation pump in the reaction loop. The loop contains a septum for gas abstraction and analysis by an HP5890 Series II gas chromatograph. Gases are introduced via a stainless steel manifold equipped with a Baratron gauge that can measure pressures between 100 mTorr and 1000 Torr. All gases are purified and can be premixed in the manifold before introduction into the reactor.

The mixing time of the chamber is about 3 min as determined by following the dilution of a plug of methane gas mix into a background of argon. The reactor volume is 62.3 l and could be pumped out to a base pressure of 5×10^{-11} Torr by opening a gate valve to an ion and turbomolecular pump. Despite the large size of the reactor, reaction rates can be measured down to 0.1 turnovers/(site $\times$ s).

The reactor is fitted with CaF_2 windows to allow infrared and visible light to pass into it and to allow sum frequency light to pass out to the detector. The sample can be resistively heated to 1000 K and cooled using liquid nitrogen to 120 K under vacuum (250 K under

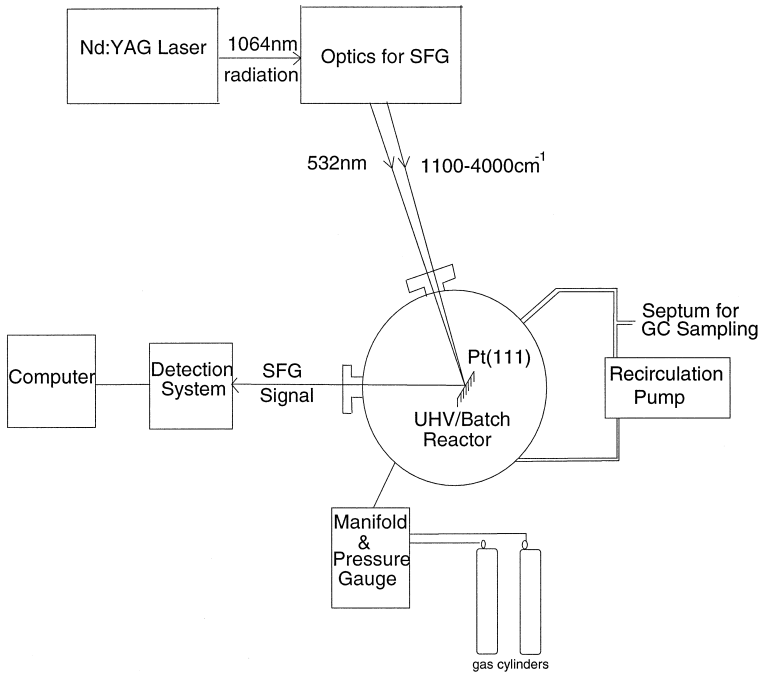

Fig. 1. The UHV/batch reactor apparatus coupled to a Nd:YAG laser for in situ SFG studies.

ambient pressure). When the reactor is under vacuum, typical surface analysis techniques such as a mass spectrometer and a retarding field analyzer for Auger and LEED are available. An Ar^+ gun allows the crystal to be cleaned by sputtering.

The laser source for the nonlinear optical experiments comes from a passive, active mode locked Nd:YAG laser which outputs a 20 ps pulse at 1064 nm when using #5 dye from Kodak. The repetition rate of the laser is 20 Hz and the total energy per pulse is approximately 50 mJ. The beam is divided into two by a beam splitter. One is frequency-doubled using KD*P to produce green light at 532 nm. The other is employed to generate tunable infrared light in the range between 1100–4000 cm^{-1} by optical parametric processes and difference frequency generation in various nonlinear optical crystals [7]. The two beams are spatially and temporally overlapped on the surface of a transition metal catalyst inside the batch reactor. The spot size of the green beam is 1.55 mm at the sample and the beam makes an angle of 50° with respect to the surface normal. The input energy is approximately 400 μJ, yielding a peak power of 0.8 GW cm^{-2}. This intensity is at least four times less than the laser damage threshold over an extended period of time. The infrared radiation is focused to approximately 1.2 mm at an angle of 56° with respect to the surface normal. Its pulse energy varies with frequency, with a maximum of 275 μJ $pulse^{-1}$ appearing at 2850 cm^{-1}.

The upcoverted light (ω_{sf}), which is in the blue (450–490 nm), is sent through a polarizer and then focused through two anti-stokes Raman edge filters onto the entrance slit of a 20-cm monochrometer. The output from the monochrometer is detected by a Hamamatsu R647-04 photomultiplier tube. The signal is converted to a voltage, sent to a box car integrator and then stored on a computer. The efficiency of the detection system is approximately 3%. The major loss of signal comes from the monochrometer (25% transmission at 460 nm) and the low quantum efficiency of the photomultiplier tube (20% at 460 nm).

2.2. SFG on single crystals of transition metals

SFG, a three-wave mixing process, is generated through the beating of input infrared (ω_{ir}) and visible (ω_{vis}) beams to produce an output at the sum frequency ($\omega_{sf} = \omega_{ir} + \omega_{vis}$) (Fig. 2) [3–6]. The visible beam is held at a fixed frequency while the infrared beam is tuned over the vibrational range of interest. The signal generated at the surface per laser pulse follows the equation [4]:

$$S(\omega_{sf}) = \frac{8\pi^3\omega_{sf}\sec^2\theta_{sf}}{\hbar c^3(\varepsilon^{sf}\varepsilon^{ir}\varepsilon^{vis})^{1/2}}|\boldsymbol{e}'_{sf}\cdot\chi^{(2)}:\boldsymbol{e}'_{ir}\boldsymbol{e}'_{vis}|^2\frac{U_{ir}U_{vis}}{AT} \quad (1)$$

Where S is the signal; $\chi^{(2)}$ is the nonlinear susceptibility of the medium being probed; ε is the dielectric constant of the probe medium; $\boldsymbol{e}'$ is a vector which describes the field polarization and has the magnitude of the Fresnel factor; U_{ir} and U_{vis} are the input infrared and visible pulse energies; A is the overlap area of the two input beams; T is the temporal overlap of the input beams; and θ_{sf} is the angle the sum frequency output makes with respect to the surface normal of the sample.

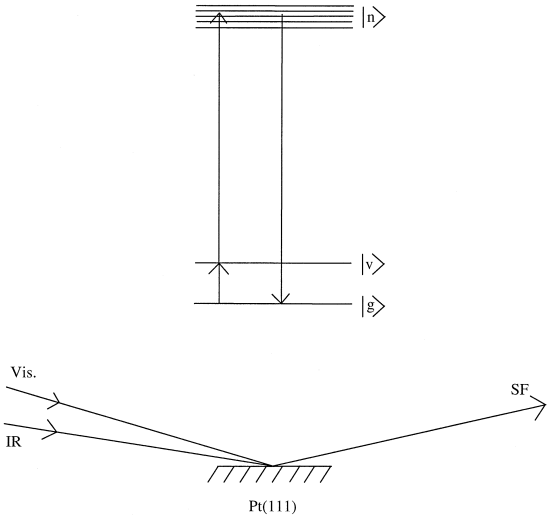

Fig. 2. The geometry of SFG from a metal surface.

A typical spectrum of a hydrocarbon species, ethylidyne ($M{\equiv}CCH_3$), on a model transition metal catalyst, Pt(111), is shown in Fig. 3a. The spectrum was taken under UHV conditions with both the infrared and visible electric fields polarized normal (or p polarized) to the surface. The sum frequency signal output was also p polarized. This is a designated PPP measurement. The peak at 2878 cm^{-1} represents approximately 7.6 counts per shot. This corresponds to more than 250 photons generated at the sample per laser shot from a nonlinearity of $|\chi|^{(2)} \approx 10^{-16}$ esu. The terms a, k, ω, θ, and Γ (shown with the spectrum) are parameters deduced from curve fitting using Eq. (1).

The PPP polarization combination consists of four possible nonzero components of the nonlinear susceptibility tensor: $\chi^{(2)}_{zzz}$, $\chi^{(2)}_{yyz}$, $\chi^{(2)}_{yzy}$, and $\chi^{(2)}_{zyy}$. Here, $\hat{z}$ is along the surface normal. The three subindices refer to the directions of the field components for SF output, visible input, and infrared beam input, respectively. However, because the field component along a metal surface is small, only $\chi^{(2)}_{zzz}$ is expected to contribute significantly to the observable signal from the PPP measurement. For the same reason, SFG signals obtained with SSP and SPS polarization combinations are expected to be weak. Fig. 3b shows the spectrum for ethylidyne on Pt(111) with the SSP polarization combination, which probes $\chi^{(2)}_{yyz}$ exclusively. The peak frequency at 2883 cm^{-1} has an intensity corresponding to approximately 0.20 photons $shot^{-1}$. This is down by a factor of 38 from the signal generated from the PPP polarization combination. Fig. 3c shows the spectrum of the same system with the SPS polarization combination. This combination probes $\chi^{(2)}_{yzy}$ exclusively. As seen from the spectrum, the signal was undetectable and therefore down by at least two orders of magnitude from the PPP spectrum. There was no detectable signal for the PSS combination either, which probes $\chi^{(2)}_{zyy}$.

The signal generated at the sample is proportional to the square of the second order susceptibility as can be seen from Eq. (1). As shown

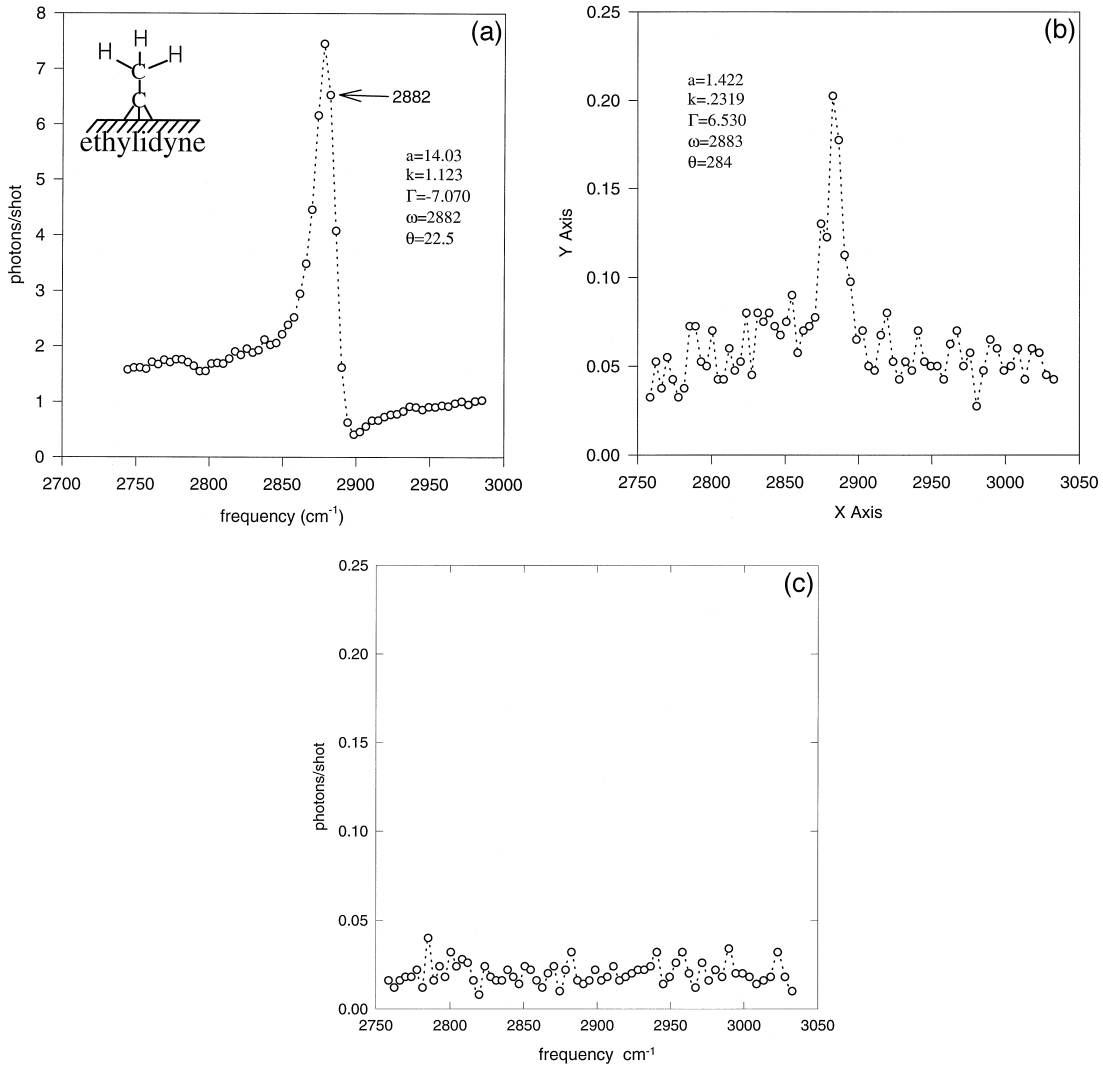

Fig. 3. The SFG spectrum of ethylidyne on Pt(111) at room temperature monitored with (a) PPP, (b) SSP and (c) SPS polarization combinations.

above, only $\chi^{(2)}_{zzz}$ contributes to the signal from a metal surface. In general, $\chi^{(2)}_{zzz}$ consists of a resonant part, $\chi^{(2)}_{\mathrm{R},zzz}$ and a nonresonant part $\chi^{(2)}_{\mathrm{NR},zzz}$. The former takes the form:

$$\chi^{(2)}_{\mathrm{R},zzz} = \sum_{\mathrm{q}} N_{\mathrm{q}} < (\hat{z}\cdot\hat{l})(\hat{z}\cdot\hat{m})(\hat{z}\cdot\hat{n}) > \alpha^{(2)}_{lmn,\mathrm{q}} \tag{2}$$

where N_{q} represents the number density of the oscillator q, *lmn* denotes the local coordinates of the oscillators, and the angular brackets describe an orientational average. The resonant nonlinear polarizability, $\alpha^{(2)}_{lmn,\mathrm{q}}$, can be written as:

$$\alpha^{(2)}_{lmn,\mathrm{q}} = \frac{A'_{\mathrm{q}}}{\omega_{\mathrm{IR}} - \omega_{\mathrm{q}} + i\Gamma_{\mathrm{q}}}$$

$$\text{and } A'_{\mathrm{q}} = \frac{1}{2\omega_{\mathrm{r}}}\frac{\partial\mu}{\partial \mathrm{q}}\frac{\partial\alpha^{(1)}_{lm}}{\partial \mathrm{q}} \tag{3}$$

Here, the resonance mode is characterized by the resonant frequency, ω_{q}, the strength A'_{q} and

the damping constant Γ_q. Note that A' is proportional to the product of two parts: the change in dipole, $\frac{\partial \mu}{\partial q}$, and the change in linear polarizability, $\frac{\partial \alpha_{lm}^{(1)}}{\partial q}$, with respect to the normal coordinate of the mode. This then constitutes the main selection rule for SFG: for a vibrational mode to be allowed in SFG, it must be both infrared and Raman active. Fortunately, for molecules adsorbed on surfaces, the lack of inversion symmetry of the surface often satisfies this selection rule.

The nonresonant contribution to the SFG signal is usually not in phase with the resonant term; we, therefore, write $\chi_{NR}^{(2)} = ke^{i\varphi}$. Since the SFG signal is proportional to $|\chi_{zzz}^{(2)}|^{(2)}$, the SFG spectrum of a system with multiple resonances is given by:

$$|\chi^{(2)}|^2 = \left| \sum_q \frac{A_q}{\omega_{IR} - \omega_q + i\Gamma_q} + ke^{i\varphi} \right|^2 \quad (4)$$

which in the case of a single resonance reduces to:

$$|\chi^{(2)}|^2 = \left| \frac{A}{\omega_{IR} - \omega_r + i\Gamma} + ke^{i\varphi} \right|^2$$

$$= \frac{A^2 + 2Ak[(\omega_r - \omega_{ir})\cos\varphi - \Gamma\sin\varphi]}{(\omega_{IR} - \omega_r)^2 + \Gamma^2} + k^2 \quad (5)$$

with A proportional to A'. The consequences of a nonresonant background are evident from Fig. 3a; it interferes with the resonant constructively at frequencies immediately to the red of the peak and destructively at frequencies immediately to the blue of the peak. This leads to the dip seen on the blue side of the resonance and a slight red shift of the peak. In Fig. 3a, for example, the peak occurs 4 cm^{-1} below the actual resonant frequency. Because of possible interferences between resonant and nonresonant contributions and between contributions from neighboring resonant modes, deduction of the number density of species on the surfaces from the SFG spectrum is a bit complex. Curve fitting of the observed spectrum using Eq. (5) is often necessary to find A_q from which N_q can then be obtained.

3. Examples of SFG studies of catalytic systems

In Sections 3.1, 3.2 and 3.3, we will discuss two specific reaction classes that have been investigated in our laboratory with infrared-visible SFG, namely olefin hydrogenation and CO oxidation. These examples are chosen to demonstrate the versatility of SFG as a tool to study heterogeneous catalysis both in UHV and under real atmospheric conditions. The results allow us to fully characterize the reaction mechanisms.

3.1. Ethylene hydrogenation

The first major system chosen for investigation involved hydrogenation of the smallest olefin, ethylene [8]. This system was chosen for its simplicity as only one product, ethane, may be formed. The majority of previous surface science studies of this system have focused on using ultrahigh vacuum conditions to analyze the nature and bonding of surface moieties formed when clean platinum surfaces are exposed to ethylene and hydrogen. It was found that in the absence of hydrogen, ethylene physisorbs to Pt(111) below 52 K [9]. This species is called π-bonded ethylene. When the surface is annealed above 52 K the π-bond of the ethylene is broken and the molecule is more strongly bound to platinum via the formation of two carbon metal sigma bonds. This species is referred to as di-σ bonded ethylene [10]. Upon further annealing of the di-σ bonded ethylene/Pt(111) system above 240 K, the adsorbed ethylene is decomposed into ethylidyne and hydrogen [11]. The identification of these surface species and others involved in hydro-

genation of ethylene can be achieved by surface vibrational spectroscopy with the help of peak assignments from known organometallic cluster analogs.

The hydrogenation of ethylene was first studied by Horiuti and Polanyi in 1938. They proposed that ethylene is hydrogenated stepwise from an adsorbed ethylene intermediate through an ethyl group to ethane. More recently, several groups have investigated the possible role of ethylidyne, knowing that it is often present on the platinum surface during the ethylene hydrogenation process. Davis et al. [12] hydrogenated ^{14}C labeled ethylidyne on Pt(111) with near atmospheric pressure of H_2. Their results indicated that the rate of hydrogenation of the ethylidyne was several orders of magnitude slower than the overall turnover rate of hydrogenation of ethylene to ethane, indicating that ethylidyne was not directly involved in the reaction. Beebe et al. [13] monitored ethylene hydrogenation over a Pd/Al_2O_3 supported catalyst in situ by using transmission infrared spectroscopy. By varying the ratio of ethylene to hydrogen it was observed that hydrogenation occurred over surfaces both with and without an ethylidyne ($\equiv CCH_3$) overlayer. Rekoske et al. [14] have repeated the transmission infrared work on Pt/Cab–O–Sil and concluded that ethylidyne was not involved in the reaction in the case of a supported platinum catalyst. All evidence strongly suggests that ethylidyne is only a spectator species in ethylene hydrogenation.

The roles of π-bonded and di-σ bonded ethylene have also been examined. Using transmission infrared spectroscopy, Mohsin et al. have shown that both π-bonded and di-σ bonded ethylene are hydrogenated when H_2 is flowed over a Pt/Al_2O_3 catalyst precovered with these species [15]. Further, they found that upon annealing a surface covered with π-bonded and di-σ bonded ethylene in the absence of hydrogen only the di-σ bonded species was converted to ethylidyne while the π-bonded ethylene remains unaffected.

None of the infrared spectroscopy studies described above, however, allowed the monitoring of surface species during ethylene hydrogenation with ethylene flowing. This is because gas phase ethylene greatly interferes with the infrared spectroscopic experiments [14]. All experiments in which di-σ and π-bonded ethylene were monitored required that ethylene be removed from the gas phase in order to make observations.

We were able to investigate ethylene hydrogenation in situ near ambient pressure and temperature using SFG spectroscopy [8]. Our results indicate that ethylene primarily hydrogenates through a π-bonded intermediate rather

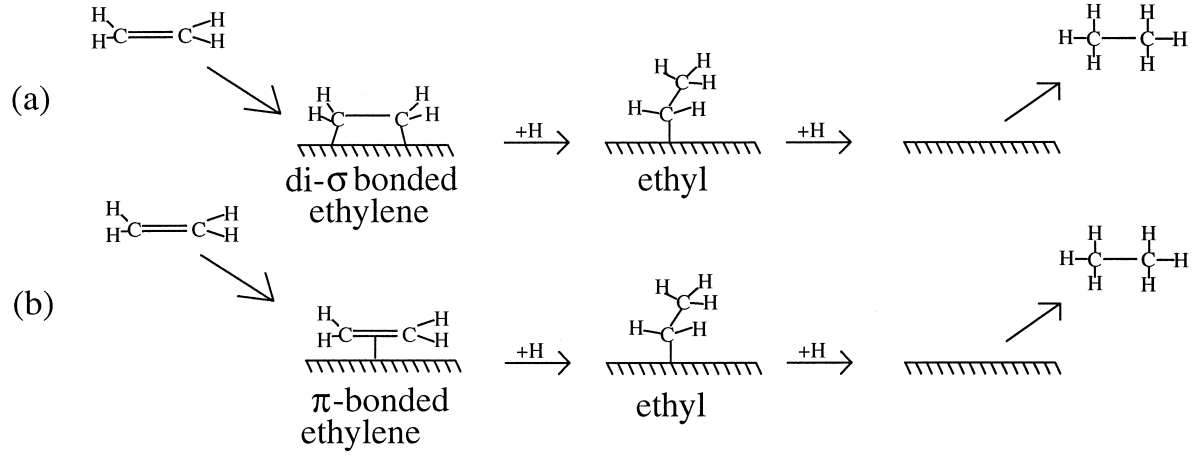

Fig. 4. Possible reaction pathways for ethylene hydrogenation.

than the more strongly adsorbed di-σ bonded ethylene species (Fig. 4). The π-bonded intermediate occupies only a few percent of surface sites during reaction and is in fast equilibrium with gas phase ethylene. Without gas phase ethylene, its presence on the surface is negligible at room temperature. This species hydrogenates through an ethyl intermediate to ethane with an identical rate in the presence or absence of ethylidyne. By contrast, di-σ bonded ethylene competes directly for sites with ethylidyne and its presence or absence had no observable effect on the reaction rate.

In our SFG study, the first step was to find vibrational spectroscopic 'fingerprints' for various surface species. This was carried out with the sample in UHV using SFG spectroscopy [16]. Fingerprint spectra of ethylidyne and di-σ bonded ethylene on Pt(111) are shown in Figs. 3 and 5a respectively. These spectra were taken

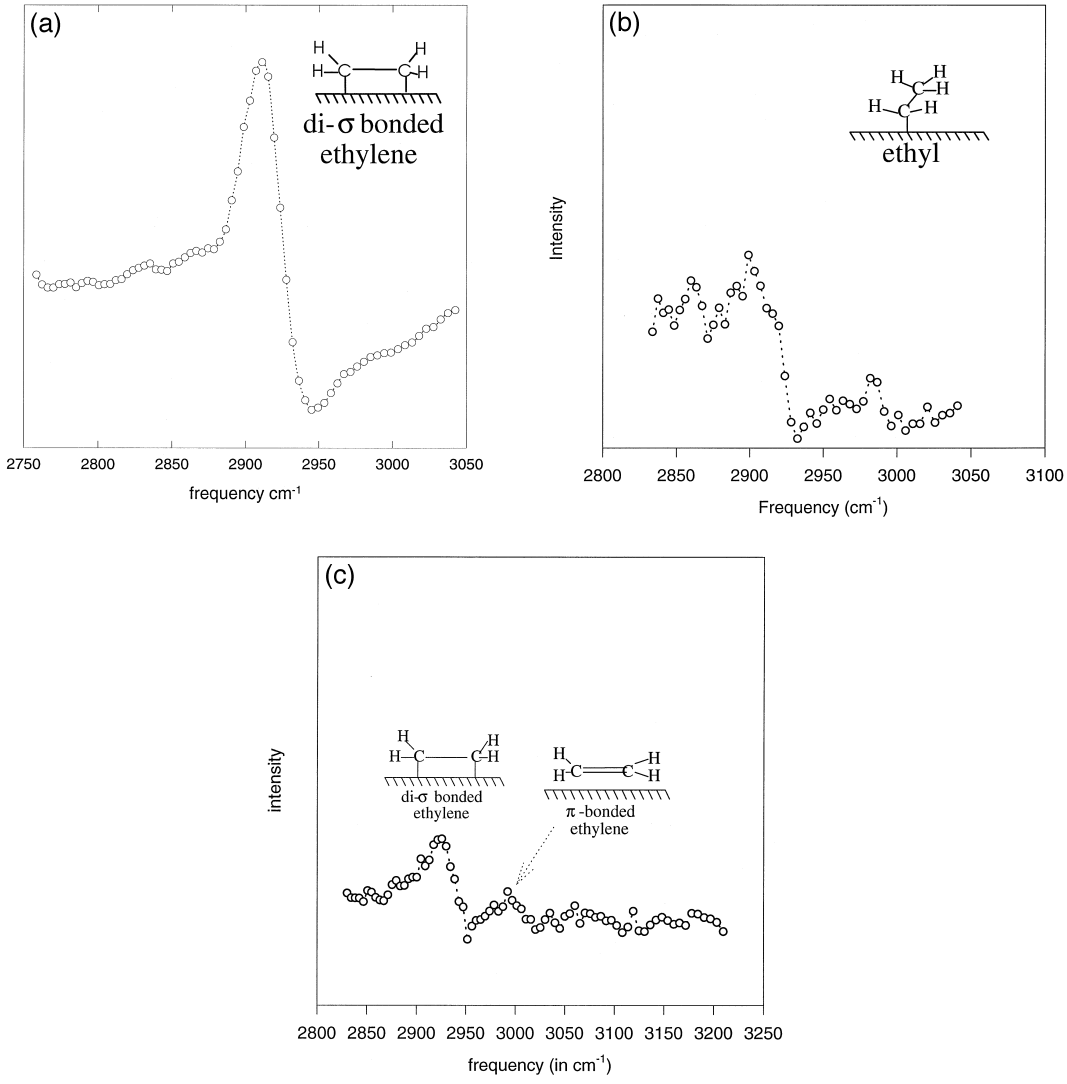

Fig. 5. Spectra of (a) a saturation coverage of di-σ bonded ethylene on Pt(111) at 200 K (b) ethyl groups formed from ethyl iodide at 193 K and (c) a mixture of di-σ and π-bonded ethylene at 120 K on O/Pt(111).

after dosing ethylene onto clean Pt(111) at 295 K for ethylidyne and 202 K for di-σ bonded ethylene. Other potentially important species such as ethyl groups and π-bonded ethylene could not be prepared by direct adsorption on clean platinum, but could be formed in the presence of other adsorbates. Ethyl groups were formed from the dissociation of ethyl iodide (Fig. 5b), while π-bonded ethylene was formed by adsorption on Pt(111) preadsorbed with oxygen (Fig. 5c).

The second step was to use these fingerprint spectra to identify the surface species present under reaction conditions and to try to find correlation or noncorrelation with the reaction rate. Fig. 6a shows the in situ SFG spectrum in the CH stretch range under reaction conditions of 100 Torr H_2, 35 Torr C_2H_4, and 615 Torr He at 295 K [8]. Under these conditions ethylene was measured to hydrogenate at a rate of 11 ± 1 turnovers per platinum site per second as determined by gas chromatography. The dominant feature in the spectrum was from ethylidyne (cover is approximately 0.18 ML). Just above the ethylidyne peak, the CH_2 symmetric stretch of di-σ bonded ethylene was observed at 2910 cm^{-1} and its coverage was nearly 0.07 ML. In addition to these two prominent features, a weak and broad hump around 3000 cm^{-1} from π-bonded ethylene was observed. The coverage of this species was about 0.04 ML based on a calibration of the well characterized $C_2H_4/O/Pt(111)$ system in UHV [17,18].

To investigate the role of various surface species in this reaction, experiments were carried out on a Pt(111) surface that was precovered with ethylidyne, prepared by dosing the clean platinum surface with 4 l of ethylene in UHV at 295 K. The crystal was then exposed to similar experimental conditions as in Fig. 6a. Fig. 6b shows the resulting vibrational spectrum. A slight increase in the ethylidyne concentration (~ 0.24 ML) and a four-fold drop in the di-σ bonded ethylene concentration (less than 0.015 ML) were observed with respect to the previous case without ethylidyne preadsorption. By contrast, the feature from π-bonded ethylene was present at nearly the same intensity as in the previous case.

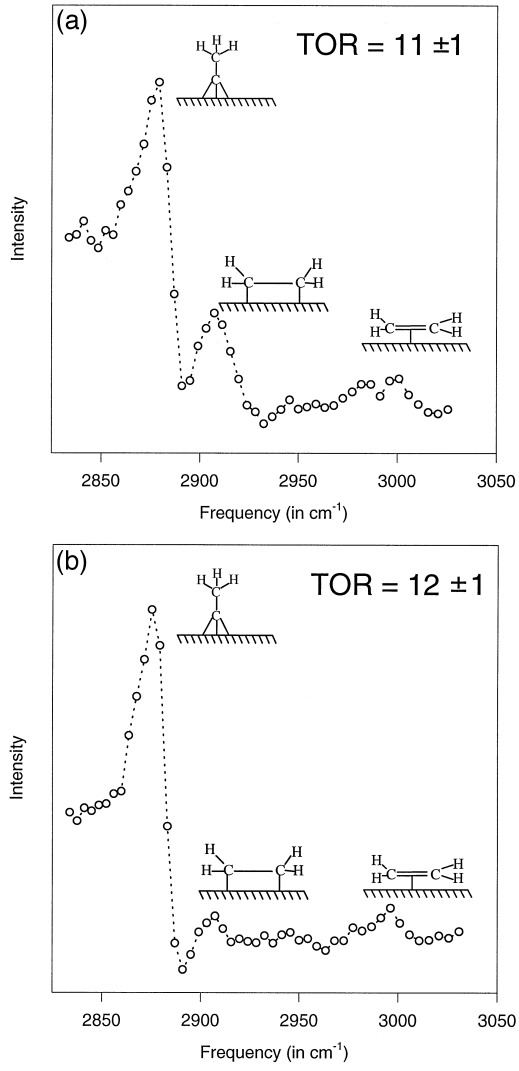

Fig. 6. (a) SFG spectrum of the Pt(111) surface during ethylene hydrogen with 100 Torr H_2, 35 Torr C_2H_4, and 615 Torr He at 295 K. (b) The SFG spectrum under the same conditions as (a), but on a surface which was precovered in UHV with 0.25 ML of ethylidyne.

The increase of ethylidyne concentration and the decrease of di-σ bonded ethylene concentration without a corresponding decrease in the rate of hydrogenation argues strongly against di-σ bonded ethylene being an important intermediate in ethylene hydrogenation. In fact, the

di-σ bonded species appear to compete directly for sites with ethylidyne. Once ethylidyne species are formed they block the adsorption sites for di-σ bonded ethylene. It is known from previous studies on supported catalyst surfaces that the presence of ethylidyne has no effect on the rate of ethylene hydrogenation [13,14]. If di-σ bonded ethylene had been an important intermediate, then ethylidyne would have been a poison for ethylene hydrogenation.

In contrast to the behavior of the di-σ bonded species, the concentration of π-bonded ethylene was unaffected by the ethylidyne concentration. Therefore, the π-bonded species is likely to be the key intermediate in ethylene hydrogenation (Fig. 4b). The strength of the π-bonded feature corresponds to approximately 4% of a monolayer; therefore, the turnover rate of the reaction at 295 K and 100 Torr H_2 is about 300 per ethylene molecule per second [19]. The above results demonstrate the difficulty in exclusively using UHV studies to characterize the mechanism for catalytic reactions. Indeed, π-bonded ethylene does not survive in vacuum near 300 K, where ethylene is typically hydrogenated. In situ studies alone are also insufficient in this case. It was important to prepare an ethylidyne covered surface in UHV in order to rule out di-σ bonded ethylene as a key reaction intermediate.

3.2. Hydrogenation of higher olefins

The hydrogenation of larger olefins represents the microscopic reverse of alkane dehydrogenation and should help aid in understanding the molecular details of olefin formation. Compared with ethylene, little UHV work has been undertaken to understand adsorption of higher α-olefins on platinum. Much of the existing work was carried out by Delacruz and Sheppard [20,21] and Sheppard and co-workers [22–

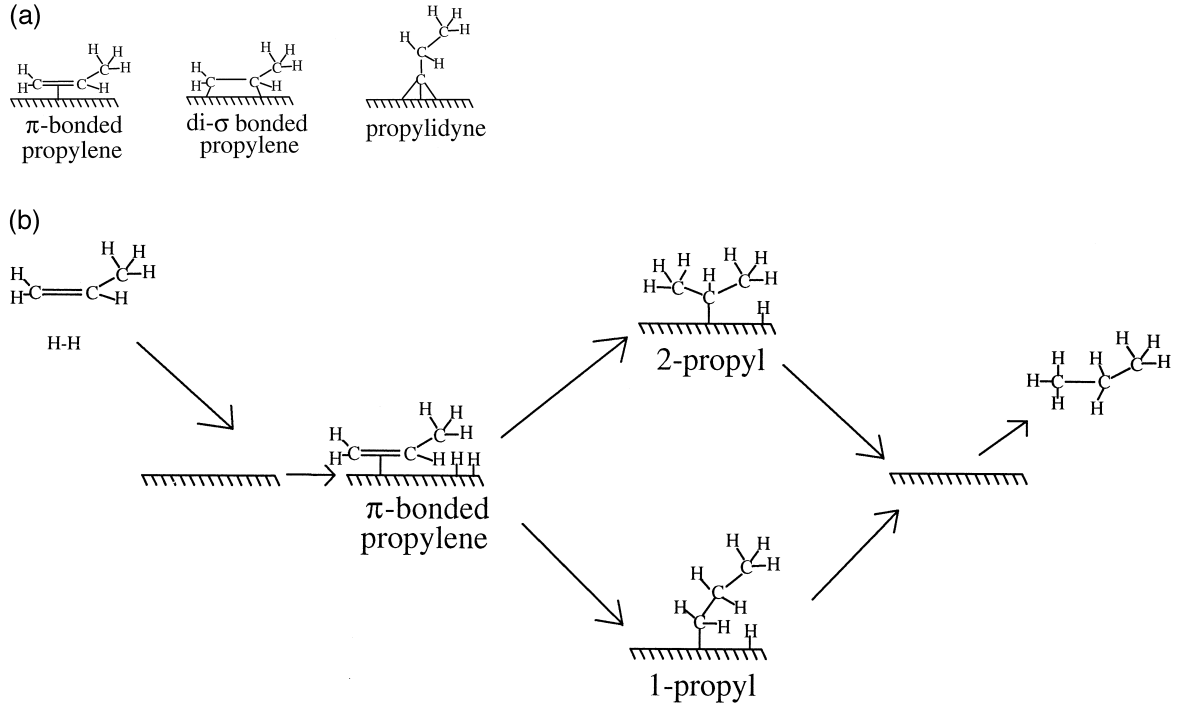

Fig. 7. (a) Propylenic moieties formed on Pt(111) (b) Possible reaction pathways for propylene hydrogenation.

24], who showed that propylene (C_3H_6) adsorbs in a di-σ bonded conformation in UHV on clean Pt(111) below 220 K [25]. Upon heating, hydrogen is evolved around room temperature and the species changes to propylidyne ($M{\equiv}CCH_2CH_3$) (Fig. 7a). These results are analogous to the formation of di-σ bonded ethylene and ethylidyne from ethylene. In fact, species corresponding to ethylenic moieties have also been found for isobutene, and 1-butene adsorbed on platinum as well [20–24]. Usually, weakly bound species (π-bonded alkenes), strongly bound species (di-σ bonded alkenes) and decomposition products (alkylidynes) are formed on the surface respectively with increasing temperature. Ex situ infrared spectroscopy of hydrogenation of higher olefins indicates that all these species can be found on a supported platinum catalyst after exposure to the olefin and hydrogen [20–24]. The hydrogenation chemistry of higher α-olefins is, however, potentially more complex than for ethylene as more possible reaction pathways to alkane production exists. This is because hydrogenation can be initiated at either the terminal or internal carbon of the double bond (Fig. 7b).

Using SFG, we found for the case of propylene hydrogenation that the reaction predominately proceeds through a 2-propyl intermediate (top pathway, Fig. 7b). Further, analogous to ethylene hydrogenation, it was found that propylene hydrogenates through a π-bonded intermediate in forming propane. It was also observed that as the size of the α-olefin grew and branched, less decomposition products were found on the surface under high pressure reaction conditions.

In obtaining the results of hydrogenation of higher olefins, the same strategy for in situ monitoring of ethylene hydrogenation was used [26,27]. Fingerprint spectra for various species were obtained with the sample in UHV and exploited for species identification at high pressure. In addition, vacuum hydrogenation studies were carried out on 1- and 2-propyl moieties. These investigations indicated that 2-propyl groups hydrogenate faster than 1-propyl groups. At high pressure 2-propyl species (dominant feature near 2840 cm^{-1}) were present at much larger concentration than 1-propyl (dominant feature near 2860 cm^{-1}) on the (111) surface of platinum when 723 Torr H_2 and 40 Torr C_3H_6 were present (Fig. 8a). The faster hydrogenation of 2-propyl species vs. 1-propyl species indicated by vacuum results in combination with the

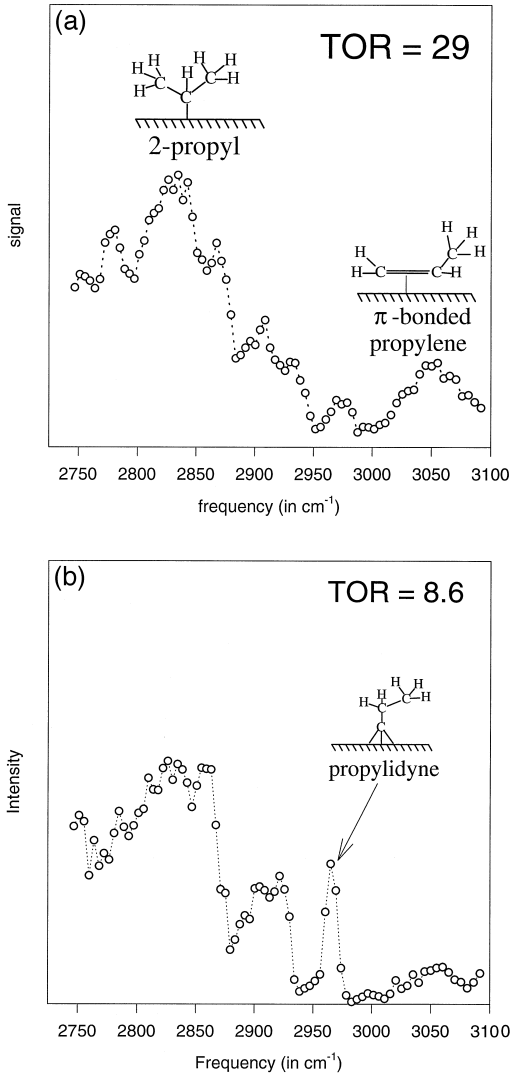

Fig. 8. SFG spectra of the Pt(111) surface during propylene hydrogenation with (a) 723 Torr H_2 and 40 Torr C_3H_6 at 295 K and (b) 100 Torr H_2, 35 Torr C_3H_6 and 617 Torr He.

predominance of 2-propyl species on the surface under hydrogenation conditions was strong evidence that the 2-propyl pathway is dominant in the formation of propane. First, the formation of 2-propyl is preferred because hydrogen addition to the terminal carbon (which is primary) is more energetically favorable than to the internal carbon (which is secondary). Second, the 2-propyl groups have a faster rate of hydrogenation than the 1-propyl groups because the Pt–C bond is weaker in the former.

As noted above, propylene hydrogenation differed from ethylene hydrogenation in the amount of carbonaceous species present on the surface during reaction. In the case of ethylene hydrogenation, ethylidyne was present on the surface near saturation coverage for conditions of 100 Torr H_2, 35 Torr C_2H_4 and 295 K (Fig. 6a). By contrast the propylidyne ($M{\equiv}CCH_2CH_3$) concentration on the surface was much less during propylene hydrogenation with 100 Torr H_2, 35 Torr C_3H_6 at 295 K (Fig. 8b). It was only about 5% of a monolayer. This trend continued for isobutene hydrogenation where no dehydrogenated species was found

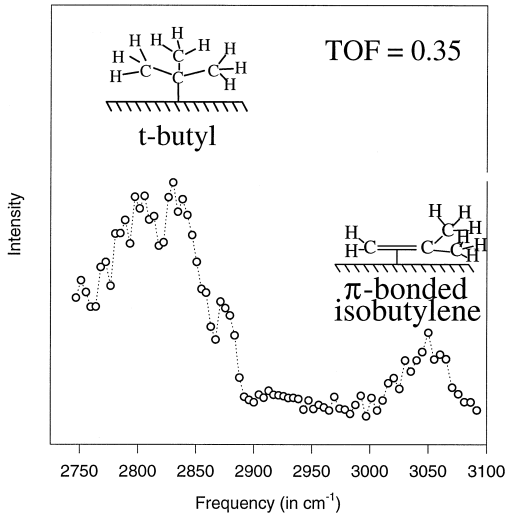

Fig. 9. SFG spectrum of the Pt(111) surface during isobutene hydrogenation with 105 Torr H_2, 40 Torr isobutene, and 635 Torr He at 295 K.

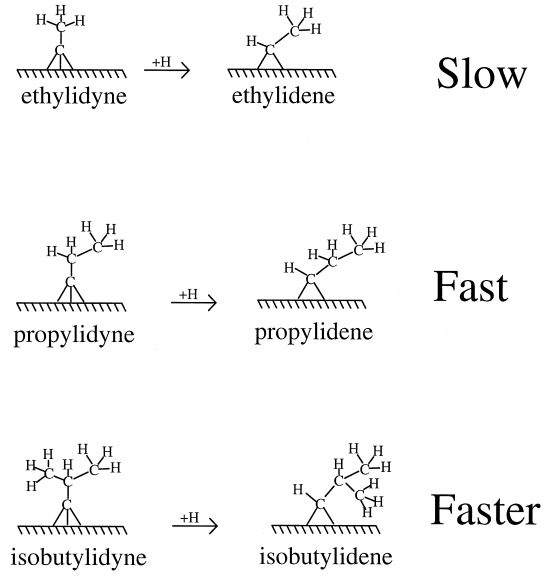

Fig. 10. A schematic representation of the hydrogenation of ethylidyne, propylidyne, and isobutylidyne to their respective alkylidenes.

(isobutylidyne would have its dominant feature at 2970 cm^{-1}) (Fig. 9).

In the case of ethylidyne, the β-carbon is primary, whereas it is secondary in propylidyne and tertiary in isobutylidyne (Fig. 10). In order to remove decomposition products from the surface, hydrogenation of these species must occur. It is likely that the first step in this process is the addition of hydrogen to the alkylidynes at the α-carbon. If the transition state for this step involves separation of charge, it is expected that a tertiary carbon at the β position would be better able to stabilize the transition state than a secondary carbon, which in turn would be better than a primary carbon. Such charge separation would occur if the transition state involved, for example, α-hydride addition. The most important consequence of the increasing hydrogenation rate with alkylidyne size is the relative degree of cleanliness that prevails on the surface under reaction conditions. Indeed, during isobutene hydrogenation with 105 Torr hydrogen, the surface was essentially free of decomposition products (Fig. 9).

3.3. CO oxidation

The oxidation of carbon monoxide to carbon dioxide has been one of the most widely investigated catalytic reactions over the past 75 years [28]. Its simplicity as well as its importance in automobile emissions control makes it an attractive topic for in situ investigation [29]. UHV studies reveal that thermal excitation of adsorbed oxygen can initiate oxidation [30]. Infrared studies have shown that atop CO species were present on the surface during carbon dioxide formation in vacuum. However, in situ infrared spectroscopy on a Pt/Al_2O_3 catalyst revealed that the density of atop CO species oscillates out of phase with the reaction rate and, hence, is unlikely to be the key surface reaction intermediate [31,32]. The success of in situ monitoring of CO oxidation with infrared spectroscopy was in part due to the substantial in-

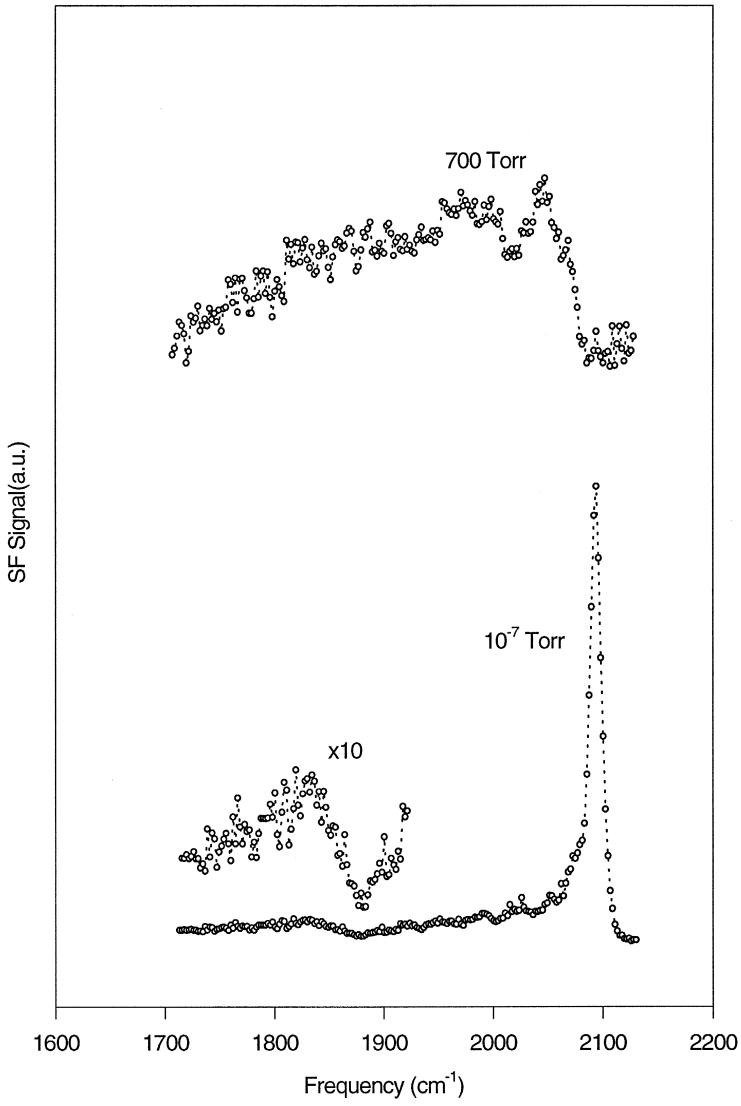

Fig. 11. SFG spectrum showing the change of surface vibrational features with increasing CO pressure.

crease in the dynamic dipole moment of an adsorbed CO species in comparison with the gas phase. Despite this, the key reaction intermediates in CO oxidation were difficult to observe using IR. Indeed, most CO oxidation studies were carried out at very low pressure [33] and the results may have little bearing on the reaction mechanism under realistic reaction conditions (ambient pressures).

Simultaneous in situ SFG and gas chromatography studies revealed that carbon monoxide oxidation took place in two distinct temperature regimes where the activation energies for CO_2 formation were dramatically different [34]. These regimes were separated by an ignition temperature above which the reaction is self-sustained without the need for heating because of the high exothermicity of the reaction. As we shall show below, SFG spectra indicate that below the ignition temperature the surface is dominated by atop CO, but above the ignition temperature it is mainly covered by incommensurately absorbed CO (i.e., highly packed CO which is out of registry with the underlying platinum atoms). In both cases, it is the coverage of incommensurate CO and not that of atop CO, that correlates with the CO oxidation rate. Clearly, incommensurate CO is the species re-

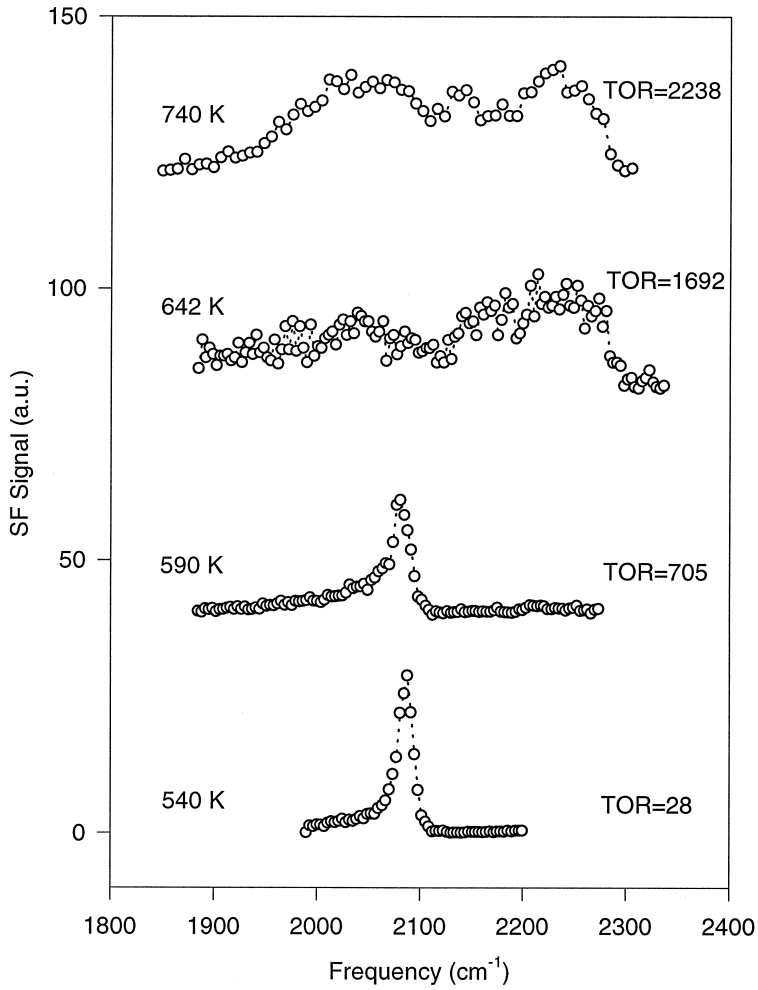

Fig. 12. Temperature dependent SFG spectra of CO oxidation on Pt(111) initially at 40 Torr CO/100 Torr O_2/600 Torr He.

sponsible for the surface catalytic reaction. In fact, atop CO is poisonous to the reaction. Below the ignition temperature, the activation energy for the catalytic reaction is found to be 42 kcal mol^{-1}, which corresponds with the desorption energy of CO. This indicates that the rate limiting step of the reaction is the desorption of atop CO. Above the ignition temperature, the atop CO hardly exists; the activation energy reduces to 14 kcal mol^{-1}, which is known to be the reaction barrier to CO and O coupling on Pt(111).

Incommensurately adsorbed CO does not exist on Pt(111) under UHV; however, its presence can easily be detected by SFG with appreciable background CO pressure [35]. Fig. 11 shows that when a clean Pt(111) surface is exposed to CO under ultrahigh vacuum, two peaks at 1845 cm^{-1} and 2095 cm^{-1}, characteristic of stretch modes of CO adsorbed on bridge and atop sites are observed (Fig. 11) [36–39]. When the CO pressure is increased to 700 Torr, the spectrum becomes dominated by a broad band extending from 1700 to 2045 cm^{-1} [35]. This broad background is apparently due to inhomogeneous broadening and can be attributed to the formation of an incommensurate CO layer on Pt(111). As the CO pressure is increased, the adsorbed species lose registry with the platinum surface atoms. High CO surface density at atmospheric pressure may also induce the relocation of surface Pt atoms, especially near defect, step, or kink sites [40]. Terminally bonded CO–Pt or even a Pt/CO binary complex, $Pt_m(CO)_n$, with n/m ratio greater than unit may also be present as judged from the appearance of a weak structure at 2045 cm^{-1} in the spectrum at 700 Torr of CO pressure.

The reaction can be followed with SFG spectroscopy and gas chromatography near atmospheric reactant pressures at temperatures ranging from 500 to 1300 K [34]. The SFG spectra of 100 Torr O_2/40 Torr CO and 600 Torr He at different surface temperatures are presented in Fig. 12. The ignition temperature, which is CO partial pressure dependent, is about 600 K for these conditions. Below ignition, atop bonded CO appears near 2095 cm^{-1} (bottom two spectra Fig. 12) and is the major species on the surface; the reaction rate is low and is inversely proportional to the surface coverage of this species (Fig. 13a). Above ignition, the SFG spectra obtained are dramatically different from those obtained below 600 K (top two spectra Fig. 12). The atop CO peak that is the dominant feature at low temperatures becomes undetectable, while three new broad bands peaked at 2045, 2130 and 2240 cm^{-1} showed up with a corresponding increase in the turnover rate to 2238 molecules per platinum site per second at 740 K. The 2130 and 2240 cm^{-1} peaks can be attributed to the stretch modes of CO adsorbed at oxidized platinum sites, which has previously been shown not to be important in CO oxidation [41]. The broad feature peaked at 2045 cm^{-1} and extending to 1700 cm^{-1} can be assigned to the incommensurate CO overlayer as we discussed earlier in connection with CO adsorption under high CO gas pressure together [35]. As

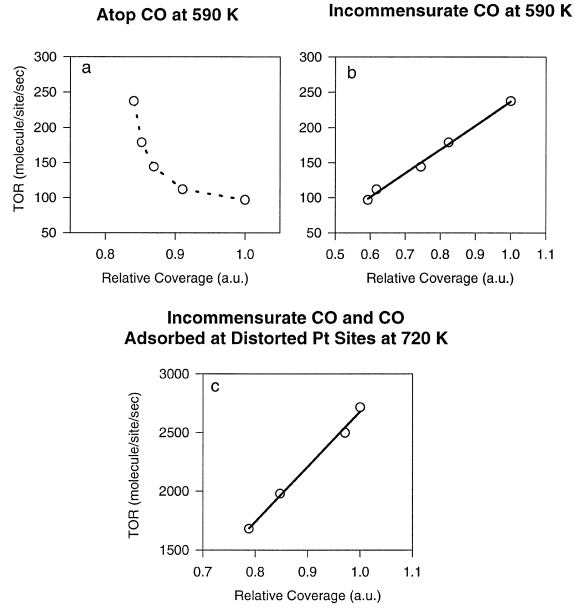

Fig. 13. Reaction rate vs. relative coverage of different surface CO species observed in CO oxidation with excess oxygen: (a) atop CO at 590 K, (b) Incommensurate CO at 590 (c) Incommensurate CO and CO adsorbed at distorted platinum sites at 720 K.

shown in Fig. 13b and c, the reaction rate is directly proportional to the coverage of this incommensurate CO species on Pt(111) at a given temperature both below and above ignition. Therefore, it is likely the species mainly responsible for the CO oxidation reaction.

We believe that the atop CO inhibits the reaction by preventing oxygen from adsorbing on Pt(111) and hence, below the ignition point desorption of the atop CO appears to be the limiting step for reaction. A small decrease in the atop CO coverage leads to a large increase in the reaction rate. Obviously, the empty atop sites left behind by CO desorption can facilitate dissociative adsorption of oxygen that will react at adjacent positions. Then without atop CO, the CO oxidation reaction is only limited by the actual reaction barrier between CO and O on the surface.

4. Future prospects

Success at applying infrared-visible SFG to in situ monitoring of high pressure reactions on model catalysts has opened up an entire new field for catalytic studies. However, at present most SFG vibrational apparatus are only capable of studying kinetics with a time resolution on the order of seconds, limiting all but the slowest reactions to batch reactor techniques. To enable in situ dynamic monitoring of surface species and permit the effects of pressure jump experiments to be observed, lasers with faster repetition rates need to be exploited. SFG spectroscopy should also be useful for studies of catalytic reactions on oxide surfaces and liquid/solid interfaces. New reactor designs will expand the number and class of reactions that could be monitored. It should be noted that in addition to SFG, other optical techniques also hold promise for in situ catalytic studies. Perhaps the most promising is polarization-modulated infrared spectroscopy [42,43]. At present, however, this technique has been mostly limited to monitoring the stretch modes of surface CO species.

Acknowledgements

This work was supported by the Director of the Office of Energy Research, Office of Basic Energy Sciences, Materials Sciences Division, of the US Department of Energy under Contract No. DE-AC03-76SF0009.

References

[1] D. Woodruff, T. Delchar, Modern Techniques of Surface Science, Cambridge Univ. Press, Cambridge, 1986.
[2] G. Somorjai, Introduction to Surface Chemistry and Catalysis, Wiley, New York, 1994.
[3] Y.R. Shen, Nature 337 (1989) 519.
[4] Y.R. Shen, Surf. Sci. 299–300 (1994) 551.
[5] X. Zhu, H. Suhr, Y.R. Shen, Phys. Rev. B 35 (1987) 3047.
[6] Y.R. Shen, The Principles of Nonlinear Optics, Wiley, New York, 1984.
[7] J. Zhang, J. Huang, Y. Shen, C. Chen, J. Opt. Soc. Am. 10 (1993) 1758.
[8] P. Cremer, X. Su, Y.R. Shen, G. Somorjai, J. Am. Chem. Soc. 118 (1996) 2942.
[9] A. Cassuto, J. Kiss, J. White, Surf. Sci. 255 (1991) 289.
[10] H. Ibach, S. Lehwald, Surf. Sci. 117 (1982) 685.
[11] H. Ibach, D. Mills, Electron Energy Loss Spectroscopy and Surface Vibrations, Academic Press, London, 1982.
[12] S. Davis, F. Zaera, B. Gordon, G. Somorjai, J. Catal. 92 (1985) 250.
[13] T. Beebe, J. Yates, J. Am. Chem. Soc. 108 (1986) 663.
[14] J. Rekoske, R. Cortright, S. Goddard, S. Sharma, J. Dumesic, J. Phys. Chem. 96 (1992) 1880.
[15] S. Mohsin, M. Trenary, H. Robota, J. Phys. Chem. 92 (1988) 5229.
[16] P. Cremer, C. Stanners, J. Niemantsverdriet, Y.R. Shen, G. Somorjai, Surf. Sci. 328 (1995) 111.
[17] H. Steininger, H. Ibach, S. Lehwald, Surf. Sci. 117 (1982) 685.
[18] A. Cassuto, M. Mane, M. Hugenschmidt, P. Dolle, J. Jupille, Surf. Sci. 237 (1990) 63.
[19] P. Cremer, X. Su, Y. Shen, G. Somorjai, Catal. Lett. 40 (1996) 143.
[20] C. Delacruz, N. Sheppard, Catal. Lett. 37 (1996) 47.
[21] C. Delacruz, N. Sheppard, J. Mol. Struct. 247 (1991) 25.
[22] G. Shahid, N. Sheppard, J. Chem. Soc., Faraday Trans. 90 (1994) 507.
[23] G. Shahid, N. Sheppard, J. Chem. Soc., Faraday Trans. 90 (1994) 513.
[24] G. Shahid, N. Sheppard, Can. J. Chem. 69 (1991) 1812.
[25] N. Avery, N. Sheppard, Proc. R. Soc. London A 405 (1986) 1.

[26] P. Cremer, X. Su, Y. Shen, G. Somorjai, J. Phys. Chem. 100 (1996) 16302.
[27] P. Cremer, X. Su, Y. Shen, G. Somorjai, J. Chem. Soc., Faraday Trans. 92 (1996) 4717.
[28] I. Langmuir, Trans. Faraday Soc. 17 (1922) 672.
[29] J. Kummer, J. Phys. Chem. 90 (1986) 4747.
[30] J. Yoshinobu, M. Kawai, J. Chem. Phys. 103 (1995) 3220.
[31] T. Lindstrom, T. Tsotsis, Surf. Sci. 150 (1985) 487.
[32] T. Lindstrom, T. Tsotsis, Surf. Sci. 171 (1986) 349.
[33] S. Hong, H. Richardson, J. Phys. Chem. 97 (1993) 1258.
[34] X. Su, P. Cremer, Y.R. Shen, G. Somorjai, J. Am. Chem. Soc. 119 (1997) 3994.
[35] X. Su, P. Cremer, Y.R. Shen, G. Somorjai, Phys. Rev. Lett. 77 (1996) 3858.
[36] N. Avery, J. Chem. Phys. 74 (1981) 4202.
[37] W. Moeher, L. Whitman, W. Ho, J. Chem. Phys. 91 (1989) 3228.
[38] H. Steininger, S. Lehwald, H. Ibach, Surf. Sci. 123 (1982) 264.
[39] B. Hayden, A. Bradshaw, Surf. Sci. 125 (1983) 787.
[40] E. Kundig, D. McIntosh, M. Moskovitis, G. Ozin, J. Am. Chem. Soc. 95 (1973) 332.
[41] J. Anderson, J. Chem. Soc., Faraday Trans. 88 (1992) 1197.
[42] B. Barner, M. Green, E. Sáez, R. Corn, Anal. Chem. 63 (1991) 55.
[43] M. Green, B. Barner, R. Corn, Rev. Sci. Instrum. 62 (1991) 1426.